Technology in Cancer Research and Treatment
ISSN 1533-0346
Volume 10, Number 6, December 2011
©Adenine Press (2011)

Near Infrared Photonic Finger Imager for Prostate Cancer Screening

www.tcrt.org

Y. Pu, Ph.D.[1]
W. B. Wang, Ph.D.[1]*
M. Xu, Ph.D.[2]
G. C. Tang, M.S.[1]
Y. Budansky, M.S.[1]
M. Sharanov, Ph.D.[1]
S. Achilefu, Ph.D.[3]
J. A. Eastham, M.D.[4]
R. R. Alfano, Ph.D.[1]*

[1]Institute for Ultrafast Spectropscopy and Lasers, Department of Physics, City College of the City University of New York, 160 Convent Avenue, New York, NY 10031
[2]Department of Physics, Fairfield University, Connecticut, CT 06824
[3]Washington University School of Medicine, 4525 Scott Avenue, St. Louis, Missouri 63110
[4]Department of Urology, Sidney Kimmel Center for Prostate and Urologic Cancers, Memorial Sloan-Kettering Cancer Center, New York, NY 10065

A portable rectal near infrared (NIR) scanning polarization imaging unit with an optical fiber-based rectal probe, designated as a Photonic Finger (PF), was designed, developed, built and tested. PF was used to image and locate the three dimensional (3D) positions of abnormal prostate tissue embedded inside normal prostate tissue. An inverse image reconstruction algorithm, namely **Op**tical **T**omography using **I**ndependent **C**omponent **A**nalysis (OPTICA) was developed to unmix the signal from targets (cancerous tissue) embedded in a turbid media (normal tissue) in the backscattering imaging geometry. The Photonic Finger combined with OPTICA was *ex vivo* tested to characterize different target(s) inside different tissue medium, including cancerous prostate tissue embedded inside large pieces of normal tissue. This new developed instrument, Photonic Finger, may provide an alternative imaging technique, which is accurate, of high spatial resolution and non-or-less invasive for prostate cancers screening.

Key words: Photonic finger (PF); Backscattering; Scanning optical polarization imaging; Optical fiber-based rectal probe; Three-dimensional localization; Human prostate tissue; Receptor-target contrast agents; Independent component analysis (ICA); Photon propagation model.

Introduction

In year 2010, 217,730 new cases of prostate cancer were diagnosed, and approximately 32,050 men died from prostate cancer in the U.S.A. (1). The common screening tests for prostate cancer diagnosis are digital rectal examination (DRE), measurement of the serum tumor marker namely prostate specific antigen (PSA), and the transrectal ultrasound (TRUS) imaging (2). A value of PSA over 4.0 ng/ml is the commonly used threshold for further diagnostic evaluation (3). Although PSA test appears to have acceptable sensitivity for late stage cancers (4) and disease with histopathologic features associated with tumor progression of a large volume, poorly differentiated cells, and extracapsular penetration (5), its accuracy is limited as low as 28%-35% (6). During the DRE, a doctor inserts a lubricated, gloved finger into the patient's rectum to feel for lumps, enlargements, or hard areas of prostate that might indicate prostate cancer. DRE has a reported sensitivity of 18%-22% (7, 8). TRUS is no longer considered as a first-line screening test for prostate cancer (9) because of its poor spatial resolution and contrast, but it does play a role in mapping the locations of the biopsy sampling (9). The confirmation of prostate cancer finally needs a needle biopsy of the prostate. In the biopsy, a number [12 to 18] of cores of prostate tissue are

Abbreviations: Photonic Finger (PF); Independent Component Analysis (ICA); **Op**tical **T**omography using **I**ndependent **C**omponent **A**nalysis (OPTICA).

*Corresponding authors:
W. B. Wang, Ph.D.
R. R. Alfano, Ph.D.
E-mail: wwang@sci.ccny.cuny.edu
ralfano@sci.ccny.cuny.edu

randomly taken from whole region of the prostate using a thin needle with the help of TRUS to map the locations of the sampling (10).

The early detection and treatment of prostate cancers can reduce mortality (11). Conventional oncology imaging methods for prostate cancer diagnosis still depend on bulk physical properties of cancer tissue and are not effective for early-stage primary tumors (12). Since PSA and DRE have limited accuracy, TRUS has poor contrast between normal and abnormal tissue regions, and needle biopsy is invasive and may cause damages of prostate, it is highly desirable to develop a better method which is accurate, of higher spatial resolution and non-or-less invasive for prostate cancer screening.

Optical imaging technique using near infrared (NIR) light provides an attractive noninvasive approach for screening human diseases. The "tissue optical window" in the NIR range, which corresponds to lower absorption from major tissue chromophores such as water, oxygenated and deoxygenated hemoglobin, allows light to penetrate deep into the tissue, up to several centimeters (12). The other main advantages of NIR optical approaches are its inherent low-cost, the ability to monitor multiple independent optical reporters simultaneously *in vivo* based upon wavelength, the absence of radioactive intermediates, and the relative simplicity of the imaging hardware as compared with Magnetic resonance imaging (MRI) and Positron emission tomography (PET) equipment. These advantages make optical imaging unmatched by any other *in vivo* imaging techniques. Over the past decade, Indocyanine Green (ICG, also called cardio-green), a clinically approved NIR dye by FDA, has been investigated as a contrast agent for optical detection of tumors. However, ICG is not designed to specifically target cancer cells. The investigations of receptor expression in normal and cancer tissues suggest that small peptide-dye conjugates can be used to target over-expressed receptors on tumors to enhance specificity (13). Biological studies have indicated that somatostatin receptors (SSTR) are over-expressed in human prostate tumor (14). The previous investigation showed that a small ICG-derivative dye-peptide, namely Cypate-Octreote Peptide Analogue Conjugate (Cytate) could be used for effectively targeting somatostatin receptor-rich tumor in the animal model because of the high affinity of Cytate for the somatostatin receptors (13). This motivates us to apply Cytate in optical scanning imaging in human prostate tissue for cancer detection. The major disadvantage of optical imaging approaches is that strong scattering by biological tissue causes most photons diffused. The very few percentage of ballistic and snake photons make direct imaging practical only in surface and subsurface layers of tissue (15, 16). Scientists have to explore optical tomography methods and/or inverse image reconstruction approaches to locate the three dimension (3D) positions of abnormal tissue or recover the 3D spatial distribution information of optical parameters of the tissue (16).

In this research, a portable rectal NIR scanning polarization imaging unit with an optical fiber-based rectal probe, named Photonic Finger (PF), was developed. The transrectal optical imaging approach was used to locate the 3D positions of abnormal prostate sites hidden in normal prostate tissue based on differences of optical parameters between cancerous and normal prostate tissues. The difference can also be enhanced using an extrinsic chromophore or fluorophore such as a receptor-targeted contrast agent. The rectal NIR scanning polarization imaging and 3D inverse location technique has potential to address the critical issues of the conventional screening methods for prostate cancer detection. The scanning polarization imaging acquires 2D images by sequentially scanning a polarized illuminating light beam at different areas of a prostate gland through rectum, and recording the distribution of light intensity backscattered from the prostate using a CCD camera. An Independent Component Analysis (ICA)-based inverse 3D location reconstruction algorithm was improved specifically for the application of backscattering configuration and used to locate the 3D positions of foreign inhomogeneities from the recorded array of the 2D images. This research provides a noninvasive optical imaging technique for detecting and 3D locating cancerous sites in prostate. Therefore, PF may introduce a new criteria/indicator for prostate cancer screening in addition to the conventional examinations to enhance the accuracy of prostate cancer detection.

Experimental Setup and Methods

Design and Construction of Photonic Finger

The Photonic Finger is a portable rectal NIR scanning polarization imaging unit with an optical fiber-based rectal probe. The unit was designed to be capable of recording sets of 2D images of the prostate by scanning the illuminating beam on the prostate through rectum walls. The major optical and electronic components of the unit include laser diodes and their power supplies, miniature scanning Galvanometric mirrors with their electronic control boards (servo driver circuit boards) and the LabVIEW control software, and illumination and imaging coherent optical fiber-bundles.

A photograph of the portable rectal NIR scanning polarization imaging unit is shown in Figure 1(A). Three diode lasers emitting at 635 nm, 750 nm, and 980 nm, respectively, are alternatively used as light sources. These wavelengths were selected to probe the native molecules such as Hb, HbO_2 and H_2O in tissues. The output beam from a laser diode is directed to the scanning galvanometric mirror system (ThorLab GVSM002 with Dual Axis Galvo Mirrors) after passing through two pinholes and a polarizer (P_1). The beam can be scanned by two miniature galvanometric mirrors in the *x*- and *y*-directions, respectively. The beam output from the galvanometric mirrors is focused using a microscopy objective

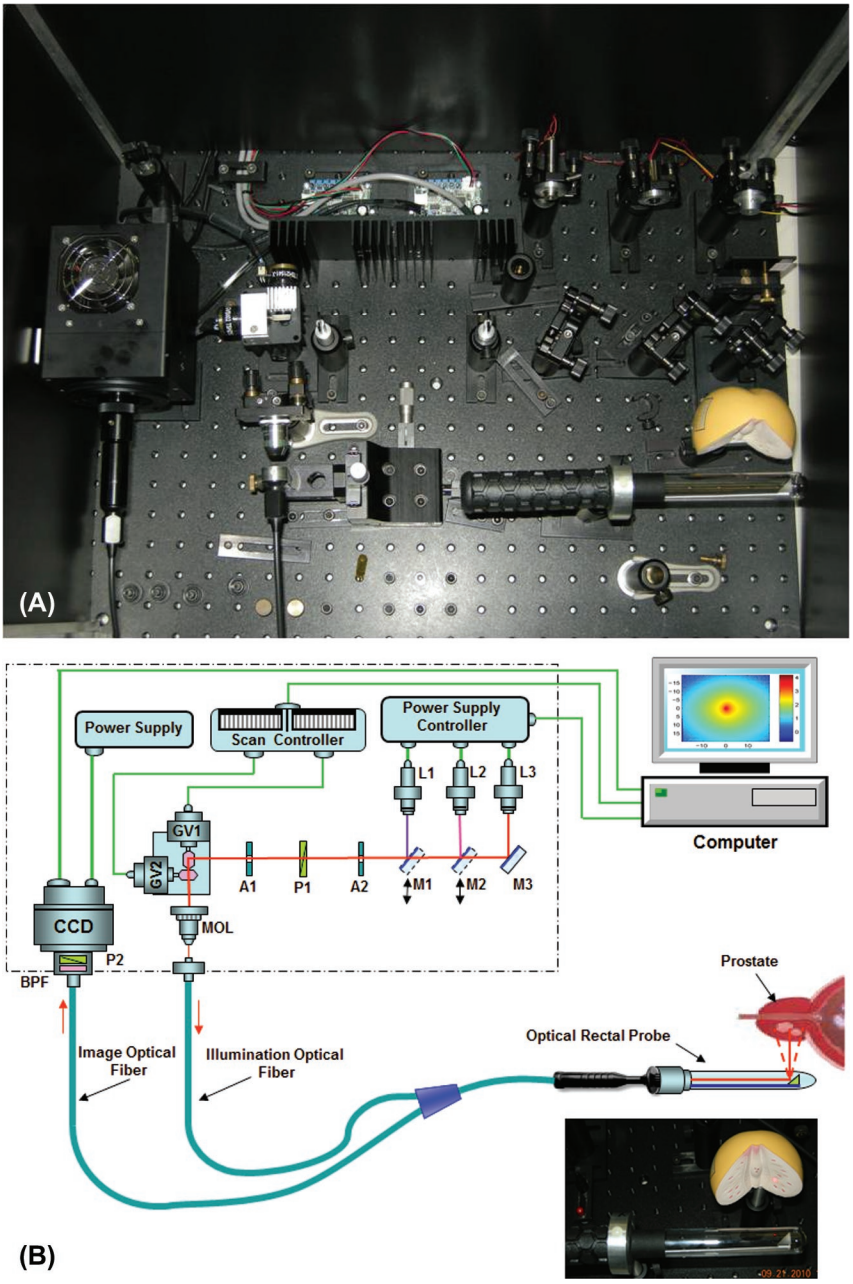

Figure 1: (**A**) A photograph of the Photonic Finger: a portable rectal NIR scanning polarization imaging unit. The power supplies and computer system are not shown in the picture. (**B**) The schematic diagram of the portable rectal NIR scanning polarization imaging unit, where L-laser, M-mirror, A-aperture, P-polarizer, GV-galvanometric scanning mirror, BPF-band pass filter, MOL-microscopy objective lens.

lens on a coherent fiber-bundle (Mytiad Fiber Imaging, 20-0826 Fiberscope Assy) used for illumination. The position of the microscopy objective lens can be adjusted in the *x*-, *y*- and *z*- three directions for the beam-fiber coupling. The output beam from the illumination fiber is directed to a small reflection prism located inside the rectal probe. The beam reflected from the prism is used to illuminate a prostate sample. This illumination beam with a diameter of ~1 mm can be scanned in the *x*- and *y*-directions on the prostate sample.

The light backscattered (or emitted) from a prostate sample is first passing through the rectal wall and reflected from the prism inside the probe head. The diameter of the probe is ~2 cm and the length is ~12 cm. The beam is then collected by a lens into another coherent fiber-bundle (Mytiad Fiber Imaging, 20-0826 Fiberscope Assy) used for imaging. The diameter of a single fiber in the bundle is ~3.2 μm each with numerical aperture N.A. ≅ 0.4. The image information formed in the optical fiber bundle was sent to a CCD camera through the coherent imaging fiber bundle and

coupling lens for recording 2D images of the prostate sample. The coupling loss of the system is ~10% and the transverse resolution is 100 μm associated with Air Force resolution target bar chart (AFBC) at group 3. A polarizer (P_2) and a band pass filter are placed in front of the CCD camera to record the 2D images at different polarization configuration and wavelengths. A cross-polarization image for each scanned illumination position of the laser beam is recorded when the polarization direction of P_2 is perpendicular to that of P_1 to suppress the contribution of light scattered (or emitted) from the surface and sub-surfaces to the images of the prostate sample. For the backscattering light imaging, a narrow band filter corresponding to the illumination wavelength is used in front of the CCD camera to ensure that the recorded images are formed only by the light backscattered from the prostate sample. For the tissue emission and/or contrast agent emission light imaging, a long pass filter is used in front of the CCD camera to ensure that the recorded images are formed only by the light emitted from the prostate sample. When the illumination light beam is scanned in the *x*-*y* plane of the sample with $n \times n$ points, an array of n^2 2D images will be recorded.

The key part of the scanning imaging unit is the scan of the illumination beam on the surface of the prostate sample with adjustable scanning parameters such as scanning area, step, speed and the number of scanning points. Figure 1(B) schematically shows the layout of the major parts and the control boards for the PF unit. This scanning system consists of (1) the Dual Axis Galvo mirrors (ThorLab GVS 002), (2) the two servo driver circuit boards and their power supply (ThorLab, GPS011), (3) the drive unit for sending voltage output to servo circuit boards (National Instruments, NI DAQmx USB-9263 USB DAQ - data acquisition), and (4) a PC with an installed LabVIEW software (LabVIEW Signal Express 2009) to power and send a command to DAQ USB 9263 to generate desired output voltage through a USB connection. In the scanning system, the drive unit NI-9263 powered by USB interface of the PC, is used to generate an analog voltage, which can be varied from −10 V to +10 V using the LabVIEW software. This analog voltage is sent to the two servo driver boards to drive the rotations of the Galvo Mirrors. For example, 1V input to the servo board can make the mirror rotate 1°. One servo board controls the X-axis, and another is for Y-axis. Both servo driver boards are powered by the power supply of GPS011. The beam scanning, the image acquiring and recording, and the synchronization of scanning and imaging are controlled by the Graphical User Interface (GUI) software developed using LabVIEW. Figure 2 shows a screenshot of the GUI after completing an $n \times n$ scan. All parameters of the scanning imaging unit (the position of the original, scanning steps, step size, exposure time, and waiting time between two adjacent imaging acquiring), can be adjusted through the GUI.

Test Samples

The Photonic Finger scanning imaging unit was tested for different types of tissue samples. The first sample used for scanning imaging was a black rubber absorber with the size of ~2.7 mm × ~3.0 mm × ~1.5 mm embedded in chicken breast tissue at different depth. The fresh chicken breast tissues were purchased at the local super market. The black rubber was covered by the chicken breast tissues at two different depths of ~5.1 mm and ~6.6 mm with a lateral dimension 38 mm × 29 mm for scanning imaging measurements. The thickness of the tissue behind the object is ~8 mm. A transport length $l_t = 1.1\,\text{mm}$ and an absorption coefficient $\mu_a = 0.007\,\text{mm}^{-1}$ were taken for chicken breast tissue for imaging analysis (17).

The second study was performed to distinguish *in vitro* cancerous prostate tissue from surrounding normal prostate tissue. Human prostate tissues were obtained from the Cooperation Human Tissue Network (CHTN) and the National Disease Research Interchange (NDRI) under the approval of the Institutional Review Board (IRB) at CCNY. The cancerous and normal prostate samples were diagnosed by pathologist before the optical imaging experiments. Samples were neither chemically treated nor were frozen prior to the experiments. The time elapsed between tissue resection and taking the scanning imaging measurements may vary for different sample sources. The longest elapsed time is about 30 hours. The sample consists of a small piece of cancerous prostate tissue (4 mm × 4 mm × 1.5 mm) embedded inside a large piece of normal prostate tissue at the depth of $z = 3.0\,\text{mm}$ from the front surface. The thickness of the whole tissue sample is 10 mm. For imaging analysis, the absorption and reduced scattering coefficients for normal prostate tissue (the host medium) were taken as $\mu_a \approx 0.026\,\text{mm}^{-1}$ and $\mu_s' \approx 0.53\,\text{mm}^{-1}$. The cancerous prostate tissue absorbs much less light with $\mu_a \approx 0.0025\,\text{mm}^{-1}$ and scatters less with $\mu_s' \approx 0.44\,\text{mm}^{-1}$ at the probing wavelength of 635 nm estimated from our earlier spectroscopic investigations of *ex vivo* prostate tissues (18). The piece of cancerous prostate tissue embedded behaves predominantly as an absorption inhomogeneity in homogeneous normal prostate tissue. Here, we simply assume that the optical parameters of normal tissue are macroscopically homogeneous throughout the tissue volume. Although this is not a rigorous description of tissue, for many cases of interest, it will be sufficient. OPTICA is applied here to extract different independent components by treating cancerous tissue as inhomogeneity embedded inside a "homogeneous" normal tissues.

The third study was designed to characterize cancerous prostate tissue after enhancing imaging contrast by extrinsic fluorescent marker, a receptor-targeted contrast agent, namely Cytate. Cytate was synthesized by Achilefu's group at the Washington

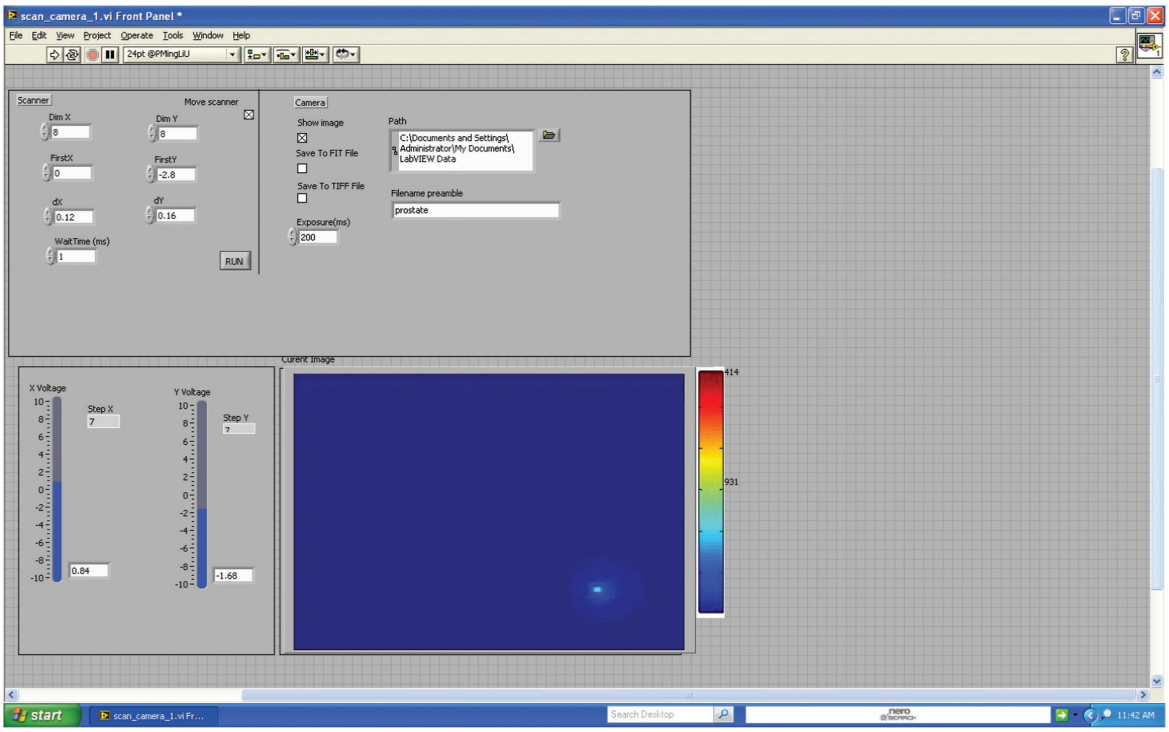

Figure 2: A screenshot of the Graphical User Interface (GUI) after completing an $n \times n$ scan. The GUI was developed using LabVIEW for operation of the Photonic Finger. All parameters of the scanning imaging (the position of the original, scanning steps, step size, exposure time, and waiting time between two adjacent imaging acquiring, *e.g.*) can be adjusted through the GUI.

University School of Medicine. This contrast agent is mainly composed of ICG and the somatostatin receptor ligand, which delivers ICG to the corresponding somatostatin receptors over-expressed in the tumor (13, 14). The prostate tissue samples for the scanning imaging study were prepared following this protocol: (1) samples (cancerous and normal prostate tissues) were cut into very tiny size, which is less than ~1 mm (in length, width and thickness) pieces. Each pair of cancerous tissue and the corresponding normal tissue used as a control sample was obtained from same patient; (2) both small pieces of prostate tissue samples were soaked in a same Cytate solution with a concentration of ~3.2×10^{-6} M for ~10 minutes; (3) Cytate-stained tissue samples were put into sodium phosphate buffer (Sigma-Aldrich) to wash off and consequently reduce the amount of un-bound Cytate (19); and (4) the Cytate-stained small pieces of cancerous and normal prostate tissues were covered by a large piece of normal prostate tissue at two different depths of ~2.5 mm and ~3.7 mm for scanning imaging measurements.

The orthogonal co-ordinate system to locate 3D positions of the target in the scanning polarized image measurements is schematically shown in Figure 3. The samples to be tested were embedded inside large slices of host tissue at different depths. The illuminating laser beam was scanned along the *x*- and *y*-directions on the front surface of the sample. The 2D images formed by the light backscattered from the sample in the normal direction are recorded. In the first and second studies, only one target (black rubber or cancerous prostate tissue) is involved in each case and the sample was illuminated by a collimated laser beam with $\lambda = 635$ nm. The elastic backscattering from the samples was collected through a narrow band filter (NF). In the third study for contrast agents' fluorescence, the Cytate-stained tiny cancerous and normal prostate tissue samples were embedded inside large pieces of normal prostate tissue. The sample was illuminated by a laser beam with $\lambda = 635$ nm in the direction close to the normal to the surface. A narrow band-pass filter at 830 nm was placed in front of a CCD camera to record emission images based on the emission peak of Cytate at ~837 nm (20).

Algorithm of OPTICA

The theory of **Op**tical **T**omography using **I**ndependent **C**omponent **A**nalysis (OPTICA) method was described in elsewhere (21). ICA, the core of OPTICA, is a solution to the *blind source separation* problems, which is a class of the problems that no precise knowledge is available on neither the mixing channels nor the sources. Typically the observations are the output of a set of sensors, where each sensor receives a set of mixed source signals (21). The algorithm of OPTICA is based on that ICA of the perturbations in the spatial intensity distributions provides the corresponding independent intensity

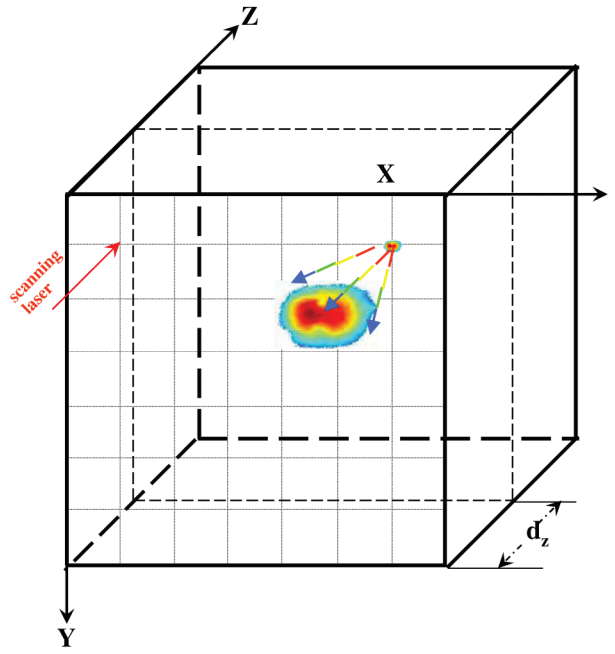

Figure 3: The schematical diagram that displays our calculated position of objects in an orthogonal co-ordinate system to locate 3D positions of the target using the scanning polarized image unit.

distributions (IID) on the detector planes (21). The measured array image is given by (16):

$$I(\boldsymbol{\rho}_d, \boldsymbol{\rho}_s) = I_0 G_0(\boldsymbol{r}_d, \boldsymbol{r}_s) - I_0 \Delta z \int G_0(\boldsymbol{r}_d; \boldsymbol{\rho}', z') \delta\mu_a(\boldsymbol{\rho}', z') G_0(\boldsymbol{\rho}', z'; \boldsymbol{r}_s)\, d^2\boldsymbol{\rho}' \quad [1]$$

where $\boldsymbol{\rho}_d$ covers the whole 2D array, $\boldsymbol{\rho}_s$ is the scanning positions of incident light source with the intensity of I_0 at the $z = 0$ plane, G_0 denotes the exact Green's function for light propagation in the host medium. It is assumed that one tiny object (with absorptive perturbation $\delta\mu_a$ of volume ΔV) is located at $r' = (\boldsymbol{\rho}', z')$ with the extension $\Delta z \ll 1$ along the axial direction and that $\delta\mu_a$ is constant within ΔV. The speed of light is set to be unity. Scattering targets can be treated in a similar fashion.

The background image could be approximately generated using an "average" image of all acquired images by shifting the scanning position for each image $\boldsymbol{\rho}_s$ to the origin 0, which is given by (16):

$$\bar{I}(\rho_d, 0) = I_0 G_0(r_d, 0) - h(\rho_d, 0) \quad [2]$$

where the term h stands for the error term. This "averaged" background image is called "dirty" background image since the object(s) with $\delta\mu_s$ and $\delta\mu_s$ is included in the averaging calculation. To generate a "clean" background image, the shifted images which are minimally perturbed by the embedded objects were selected and averaged (16):

$$\bar{I}_c = \bar{I}(\rho_d, 0) + h(\rho_d, 0) \quad [3]$$

where the error term is chosen by:

$$h(\rho_d - \rho_s, 0) = \frac{1}{N_B} \sum_{\rho_s \in B} \Delta I(\rho_d - \rho_s, 0) \quad [4]$$

where B denotes the perimeter of the scanning grid which contains N_B scanning positions. After h and the clean image of the host medium have been obtained, the difference images are calculated more accurately (16) since the cleaning imaging suppresses the contributions from embedded objects (cancerous tissues) to simulate a more "homogeneous" background.

The difference images were then generated by subtracting the "clean" background image from the recorded 2D images. Based on the difference images, ICA was used to unmix the signal arising from individual targets and the independent intensity distribution due to the target(s). Each target is associated with one independent component (IC), which consists of the projection of the Green's functions, $G_0(\boldsymbol{r}_s, \boldsymbol{r}_t)$ and $G_0(\boldsymbol{r}_d, \boldsymbol{r}_t)$, on the source or detector plane, respectively (21). The position of the target is obtained by numerically marching the target(s) to the surface until matching the retrieved independent component, incorporating both the beam profile and the surface property of the sample (14). The 3D locations of a black rubber hidden inside chicken breast tissue medium, and 3D locations of a small piece of cancerous prostate tissue embedded in the host normal prostate tissue were used to verify our new OPTICA algorithm using the recorded sets of 2D backscattering images. The procedures of OPTICA for obtaining 3D locations of objects in scattering media are listed in Table I.

Table I

Steps of OPTICA to locate 3D position of target(s) inside scattering medium at backscattering configuration.

1. Record a set of images with embedded inhomogeneities at different illuminated scanning positions;
2. Generate a "clean" background image from the "dirty" background image produced by selecting and averaging the minimally perturbed images;
3. Calculate the difference images between the recorded images and the "clean" background image;
4. Do ICA analysis of the set of difference images to generate the Independent Components (ICs);
5. Obtain the contribution of each target to intensity distribution;
6. Estimate 3D location of the target relative to boundaries by numerically marching the target to the surface until matching the retrieved IC.

Experimental Results

To illustrate the procedures and improvement of OPTICA using PF particularly developed for backscattering geometry, a set of scanning optical polarized images of a small piece of cancerous prostate tissue embedded in normal prostate tissue were acquired by the Photonic Finger. Figure 4 shows the typical scanning images chosen from the total 8 × 8 polarized images recorded by scanning the incident beam on the *x*-*y* plane of the sample. The images shown on the four corners [images (1, 1), (1, 8), (8, 1), (8, 8)] are chosen by the *x*-*y* positions of the incident light far from the embedded object while other images in the central area [images (3, 5), (3, 6), (4, 5), (4, 6)] are chosen by the *x*-*y* positions of the incident light close to the embedded cancerous tissue. There is no big difference of the light intensity distribution pattern among these recorded images except the position at the maximum intensity. This is because of the sharp peak of light intensity scattered from the surface and subsurface in the backscattered direction (16), which suppresses the perturbation caused by $\delta\mu_a$ and/or $\delta\mu_s'$ from the embedded cancerous tissue. To overcome this difficulty, a "clean" background image (CBI) needs to be synthesized. In "clean" background image synthesis, the incident light position of each of 8 × 8 images is set to origin. All array images are then shifted to the origin and the size of each image is cropped at the boundary while incident light distribution reaches the noise level. The images minimally perturbed by the embedded targets are selected for synthesizing the "clean" image.

After the "clean" background image is obtained, the perturbation 2D (*x*-*y*) images are generated by extracting the "clean" background image from the recorded images. In the perturbation 2D images, the perturbation caused by the embedded cancerous tissue was highlighted. ICA is then performed upon the perturbation images to recognize leading independent components (ICs). Each target is associated with one independent component (IC). As an example, Figure 5 shows the OPTICA-generated independent intensity distributions of a cancerous prostate tissue embedded in normal prostate tissue. Figure 5(A) is for the leading independent component, and Figure 5(B) is for residual (noise) component. It is clear that the existence of target (the cancerous prostate tissue) can be discerned from Figure 5(A). The *x*- and *y*-locations of the cancer tissue can be obtained from the position of maximum intensity of Figure 5(A). The signal strength of Figure 5(A) is much stronger than that of Figure 5(B), indicating

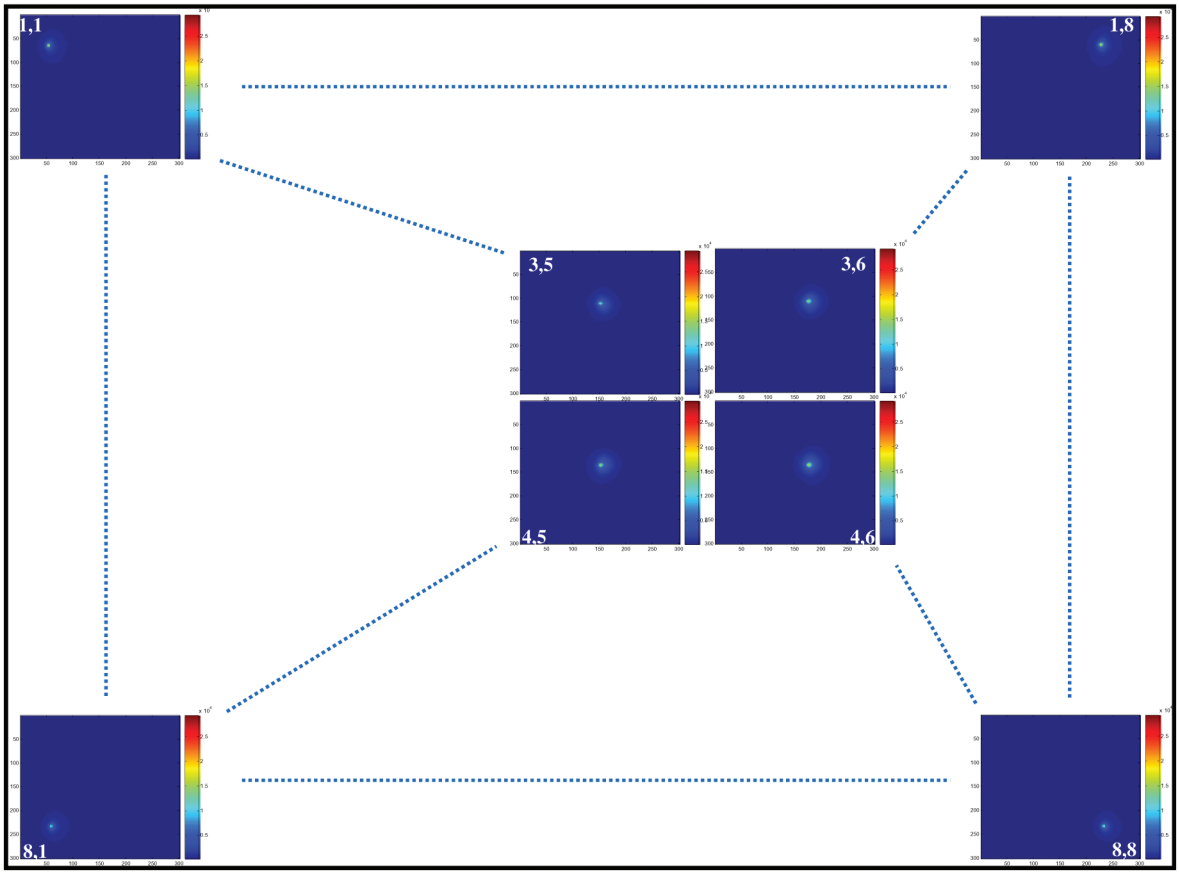

Figure 4: A set of 64 (8 × 8) images recorded by scanning the incident beam on the *x*-*y* plane of the sample (a small piece of cancerous prostate tissue hidden in the host normal tissue).

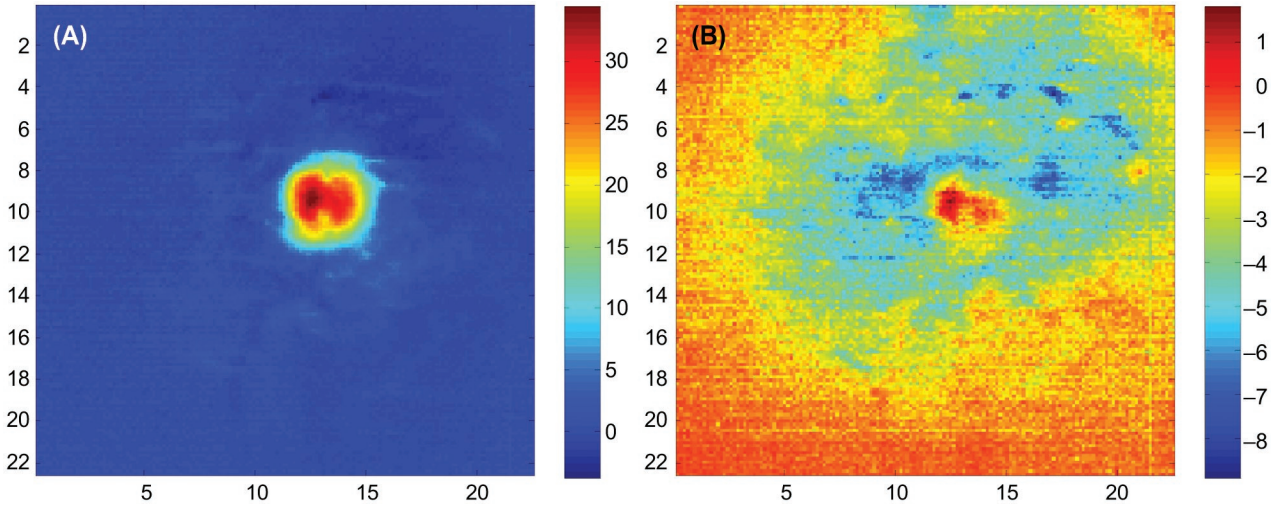

Figure 5: OPTICA-generated intensity distributions of the independent components on the detector plane for the sample consisting of a small piece of cancerous prostate tissue embedded in normal prostate tissues. (**A**) is the leading IC; and (**B**) is the residual (noise) component.

independent intensity distribution in Figure 5(A) generated by OPTICA is the leading IC. The OPTICA-generated intensity distributions of the leading independent component(s) on the detector plane can be used to locate the z-position of the cancerous tissue by numerical matching the target to the surface of the medium until matching the retrieved IC. (14). The result of $z = 3.1$ mm obtained from OPTICA analysis is in good agreement with the actual depth of ~3 mm.

The OPTICA-generated independent components using data of the scanning fluorescent images of Cytate-stained cancerous and normal prostate tissues embedded in large normal prostate tissue are shown in Figures 6(A) to 6(F). Figure (A) and (B) show the first leading IC standing for Cytate-stained cancerous tissue location; (C) and (D) show the second IC indicating Cytate-stained normal tissue location; (E) and (F) show residual – noise. The 3D locations of the Cytate-stained cancerous prostate tissues were obtained using similar methods described above.

OPTICA-generated results are summarized in Table II under different conditions using backscattering polarized imaging and OPTICA, which lists the OPTICA-determined positions of different objects in the different experiments mentioned above in comparison with their known 3D locations.

Another salient feature shown in Figure 6 is the higher emission intensity of the stained cancerous tissue compared to the stained normal tissue. This is attributed to the preferential uptake of Cytate by cancerous prostate tissue (12, 17-19). Using the data shown in Figure 6, the ratio of I_c/I_n after OPTICA analysis was found to be ~3.9 and ~2.3, for the samples with depths of 2.5 mm and 3.5 mm, respectively.

Discussion

Prostate cancer is classified as an adenocarcinoma, or glandular cancer which is developed from epithelial cells (22). About 70% of prostate cancer arises in the peripheral zone (22). The mean mucosa thickness of 830 ± 60 μm and the mean rectal wall thickness of 2.57 ± 0.15 mm (22, 23) allows the NIR scanning laser beam to penetrate the rectal wall to reach prostate for optical imaging through rectum (12, 24). By employing scanning NIR imaging, Photonic Finger can be used to characterize cancerous prostate tissue up to ~3 mm

Table II
Comparison of the known and OPTICA determined positions of embedded objects.

Object	Covered tissue	Known (x, y, z) position (mm)	OPTICA-generated (x, y, z) position (mm)
Cancerous prostate tissue	Normal prostate tissue	(13.5, 10.1, 3.0)	(13.8, 10.3, 3.1)
Stained cancerous tissue	Normal prostate tissue	(17.8, 14.6, 2.5)	(17.9, 14.4, 2.3)
Stained cancerous tissue	Normal prostate tissue	(18, 24, 3.5)	(17.6, 23.8, 3.6)
Black rubber	Chicken tissue	(15.6, 10.4, 5.1)	(15.2, 10.2, 4.7)
Black rubber	Chicken tissue	(15.6, 10.4, 6.6)	(15.3, 10.8, 6.2)

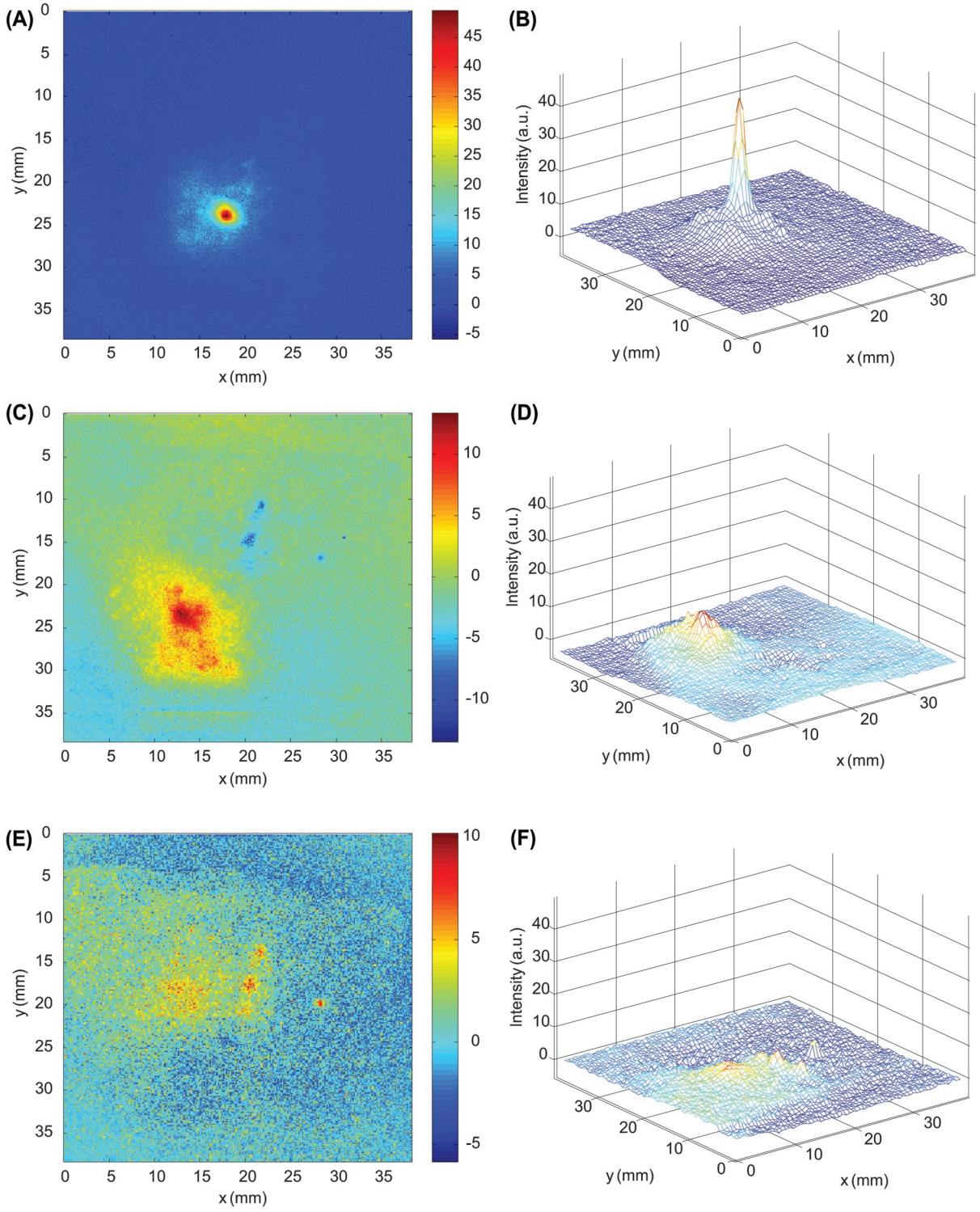

Figure 6: OPTICA-generated intensity distributions of the independent components on the detector plane for the sample consisting of the Cytate-stained cancerous and normal prostate tissues embedded in normal prostate tissue. (**A**) and (**B**) show the first leading IC indicating for Cytate-stained cancerous prostate tissue; (**C**) and (**D**) show the second leading IC standing for Cytate-stained normal prostate tissue; and (**E**) and (**F**) show the residual (noise) component.

without contrast agents. With the enhancement of the receptor-target contrast agent, PF can detect cancer at much deeper tissue layer. Previous spectral polarized imaging experiments performed in IUSL show that ICG-stained small object hidden inside the host prostate tissues in the rectum-membrane-prostate structures at depths of 7.5 mm can be imaged and

identified using fluorescence imaging methods (25). ICG is the fluorescent part of Cytate. It is reasonable to assume that PF can detect cancer in deep prostate tissue layer more than 7.5 mm under optimal condition with the enhancement of the receptor-target contrast agent. The PF will achieve diagnostic function as a screening tool other than TRUS. It is well known that TRUS alone cannot be considered as a screening tool for prostate cancer detection (9). It is used as location map when numbers of biopsy samples were taken randomly from the prostate using biopsy needles of ~1.2 millimeters in diameter (25). The number of biopsies that should be performed is debated. Twelve or eighteen biopsies suggested by different protocols were reported (22). The oversampling and overtreatment of prostate cancer is now a great concerning in prostate cancer research (22, 25) not only because of the increased numbers of sampling will cause bleeding and pain, but also because the penetration and bleeding may cause the metastasis of prostate cancer to other organ (22, 25). In contrast to TRUS, Photonic Finger can locate the 3D positions of cancerous prostate sites. Therefore, it may function as a detecting and screening instrument. Photonic Finger, an optical scanning imaging system may have positive impact in clinic applications to reduce significant pain and amount of bleeding for patients in prostate cancer detection.

Conclusion

In conclusion, a portable rectal NIR scanning polarization imaging unit with an optical fiber-based rectal probe, named Photonic Finger, was designed, developed, assembled and tested on *ex vivo* tissues at IUSL in CCNY. This instrument combined with OPTICA was achieved to characterize and 3D-locate cancerous prostate tissue embedded in normal prostate tissue in backscattered geometry for the first time. The retrieved 3D locations are in good agreement with the known position of the embedded object. This technique was able to sense weak/small absorptive, scattering, or fluorescent inhomogeneities. This new developed Photonic Finger instrument may provide an alternative imaging technique for prostate cancer detection, which is accurate, of higher spatial resolution and non-or-less invasive, and can be applied in near-real-time for *in-vivo* detection.

Acknowledgement

This research is supported by U. S. Army Medical Research and Material Command (USAMRMC) grant of W81XWH-08-1-0717(CUNY RF # 47170-00-01). Y. Pu acknowledges additional support from the USAMRMC grant of W81XWH-11-1-0335 (CUNY RF # 47204-00-01), and M. Xu acknowledges additional support from USAMRMC grant of W81XWH-10-1-0526 and NIH (1R15EB009224). The authors acknowledge the help of CHTN and NDRI for providing normal and cancerous prostate tissue samples for the measurements.

Reference

1. American Cancer Society, Cancer Facts & Figures 2010, *Atlanta: American Cancer Society* (2010).
2. Abrahamsson, A., Bostwick, D. The biological nature of prostate cancer – a basis for new treatment approaches. http://www.urologi.org/sota/STA026/sta26app.pdf
3. Optenberg, S. A., Thompson, I. M. Economics of screening for carcinoma of the prostate. *Ural Clin North Am 17*, 719-737 (1990).
4. Gann, P. H., Hennekens, C. H., Stampfer, M. J. A prospective evaluation of plasma prostate-specific antigen for detection of prostate cancer. *JAMA 263*, 289-294 (1995).
5. Mettlin, C., Mruphy, G. P., Lee, F., *et al.* Characteristics of prostate cancer detected in the American Cancer Society National Prostate Cancer Detection Project. *J Urol 152*, 1737-1740 (1994).
6. Catalona, W. J., Smith, D. S., Ratliff, T. L., Dodds, K. M., Coplen, D. E., Yuan, J. J., Petros, J. A., Andriole, G. L. Measurement of prostate specific antigen in serum as a screening test for prostate cancer. *N Engl J Med 324*, 1156-1161 (1991).
7. Catalona, W. J., Richie, J. P., Ahmann, F. R., *et al.* Comparison of digital rectal examination and serum prostate specific antigen in the early detection of prostate cancer: results of a multi-center clinical trial of 6,630 men. *J Urol 151*, 1283-1290 (1994).
8. Vihko, P., Kontturi, O., Ervast, J., *et al*. Screening for carcinoma of the prostate: rectal examination and enzymatic radioimmunologic measurements of serum acid phosphatase compared. *Cancer 56*, 173-177 (1985).
9. Ferrini, R., Woolf, S. H. Screening For Prostate Cancer in American Men. http://www.acpm.org/prostate.htm, *American College of Preventive Medicine – Practice Policy Statement.*
10. Tindall, D. J., Scardino, P. T. Defeating prostate cancer: Crucial direction for research — except from the report of the Prostate Cancer Progress Review Group (Review). *Prostate 38*, 166-171 (1999).
11. Catalona, W. J., Smith, D. S., Ratliff, T. L., Basler, J. W. Detection of organ-confined prostate cancer is increased through use of prostate-specific antigen-based screening. *JAMA 270*, 948 (1993).
12. Pu, Y., Wang, W. B., Tang, G. C., Zeng, F., Achilefu, S., Vitenson, J. H., Sawczuk, I., Peters, S., Lombardo, J. M., Alfano, R. R. Spectral polarization imaging of human prostate cancer tissue using a near-infrared receptor-targeted contrast agent, *Technol Cancer Res Treat 4*, 429-436 (2005).
13. Achilefu, S., Dorshow, R. B., Bugaj, J. E., Rajagopalan, R. Novel receptor-targeted fluorescence contrast agent for *in vivo* tumor imaging. *Investigative Radiology 35*, 479-485 (2000).
14. Hansson, J,, Bjartell, A., Gadaleanu, V., Dizeyi, N., Abrahamsson, P. A. Expression of somatostatin receptor subtypes 2 and 4 in human benign prostatic hyperplasia and prostatic cancer. *Prostate 53*, 50-59 (2002).
15. Wang, L., Ho, P. P., Liu, C., Zhang, G., Alfano, R. R. Ballistic 2-D imaging through scattering wall using an ultrafast Kerr gate. *Science 253*, 769-771 (1991).
16. Pu, Y., Wang, W. B., Tang, G. C., Budansky, Y., Alfano, R. R., Xu, M. Backscattering scanning optical imaging with independent component analysis: three-dimensional localization of objects in tissue., *Proceedings of SPIE 7895*, pp. 78950K-1-5 (2011), in the "Optical Biopsy IX", BO206, edited by R. R. Alfano and Stavros G. Demos.
17. Cheong, W. F., Prahl, S. A., Welch, A. J. A review of the optical properties of biological tissues. *IEEE J Quantum Electron 26*, 2166-2185 (1990).
18. Pu, Y. Fractal dimensional parameters and optical coefficients of cancerous and normal prostate tissues. A dissertation thesis of the City University of New York, Chapter 3, 48-76 (2010).
19. Pu, Y., Wang, W. B., Das, B. B., Achilefu, S., Alfano, R. R. Time-resolved fluorescence polarization dynamics and optical Imaging of Cytate: a prostate cancer receptor-targeted contrast agent. *Applied Optics 47*, 2281-2289 (2008).

20. Pu, Y., Wang, W. B., Achilefu, S., Alfano, R. R. Study of rotational dynamics of receptor-targeted contrast agents in cancerous and normal prostate tissues using time-resolved picosecond emission spectroscopy. *Applied Optics 50*, 1312-1322 (2011).
21. Xu, M., Alrubaiee, M., Gayen, S. K., Alfano, R. R. Optical imaging of turbid media using independent component analysis: theory and simulation. *J Biomed Opt 10(5)*, 051705-1-12 (2005).
22. Theodorescu, D., Krupski, T. L. Prostate cancer – biology, diagnosis, pathology, staging, and natural history. http://emedicine.medscape.com/article/458011-overview, May 21 (2009).
23. Huh, C. H., Bhutani, M. S., Farfan, E. B., Bolch, W. E. Individual variations in mucosa and total wall thickness in the stomach and rectum assessed via endoscopic ultrasound. *Physiol Meas 24*, N15-N22 (2003).
24. Wang, W. B., Ali, J. H., Alfano, R. R., Vitenson, J. H., Lombardo, J. M. Spectral polarization imaging of human rectum-membrane-prostate tissues. *IEEE Journal of Selected Topics in Quantum Electronics 9*, 288-293 (2003).
25. Dr. Tom. Urologist. "Men's Prostate Biopsy", http://www.articlesbase.com/advertising-articles/men039s-prostate-biopsy-1925566.html

Received: June 14, 2011; Revised: August 15, 2011; Accepted: August 24, 2011